ADVANCED FUNCTIONAL MATERIALS
www.afm-journal.de

Diamond Surfaces with Air-Stable Negative Electron Affinity and Giant Electron Yield Enhancement

Kane M. O'Donnell, Mark T. Edmonds, Juergen Ristein, Anton Tadich, Lars Thomsen, Qi-Hui Wu, Chris I. Pakes, and Lothar Ley*

The presence of an air-stable negative electron affinity (NEA) on lithium-covered oxygen-terminated diamond after a thermal activation process is demonstrated. The NEA is unequivocally established by the onset of photoelectron yield at the bandgap energy of 5.5 eV. This surface exhibits a secondary electron yield enhancement by a factor of 200, compared to a surface with positive electron affinity. The surface chemistry leading to the necessary surface dipole was elucidated by core-level photoemission spectroscopy in conjunction with previous theoretical calculations. The insensitivity to the details of the deposition process opens a route to practical and robust negative-electron affinity devices based on diamond.

1. Introduction

There are a number of applications such as photocathodes in image intensifiers or cathodes for vacuum electronics,[1] electron amplifiers,[2] and thermionic converters[3,4] where a high emission probability of electrons is required. All other things being equal, the emission probability is greatly enhanced if the electrons are not hindered by emission barriers as they occur for metals in the form of the work function or in semiconductors in the form of a positive electron affinity (EA). The latter measures the energy required to emit an electron from the conduction band minimum (CBM) to the vacuum level E_{VAC}. While the metal work function cannot be made to disappear, there are many ways to reduce or even eliminate the emission barrier in semiconductors. This is commonly achieved by chemical modifications of the surface, such that a dipole layer is formed in a way that the dipole potential lowers E_{VAC} relative to the CBM. If this lowering is combined with a strong downward band bending at the surface such that E_{VAC} lies below the bulk CBM (i.e., the CBM is beyond the space charge region) one speaks of effective negative electron affinity. In this case, electrons at the CBM approaching the surface have a certain probability to tunnel through the space charge region, maintain their original energy and escape into vacuum without encountering a barrier (ballistic electron emission). This recipe is followed, for example, by modern photo cathodes where a surface layer of oxidized Cs forms the dipole layer and serves at the same time to provide the doping necessary to induce the strong downward band bending at the GaAs surface.[5,6] Much more efficient electron emitters are to be expected when true negative electron affinity (NEA) is achieved, that is, when the vacuum level lies below CBM right at the surface. To our knowledge, hydrogen-terminated diamond is so far the only inorganic semiconductor where true NEA has been reproducibly observed.[7–10] For the hydrogen-terminated C(100):H and C(111):H surfaces EAs of –1.3 eV have been reported, and the mechanism behind this low EA relies on the high dipole density formed by the polar C–H surface bonds; it turns the already small electron affinity of the clean diamond surface (0.3 eV) into true NEA.[9,10]

As expected, the electron emission probability of C(100):H is far superior to that of unhydrogenated diamond. Cui et al. measure a rise in photo induced electron yield by five orders of magnitude when the surface turns from positive electron affinity (PEA) to NEA.[11] The reason lies in the difference in electron collection depth by the same ratio. For PEA, only electrons that exceed the CBM by an energy equal to the EA are able to escape. These "hot" electrons, however, have a very short inelastic mean free path of a few nanometers, on account of their fast thermalization rate that lies in the 10^{12} sec^{-1} range. Without a barrier, thermalized electrons contribute to the yield and their mean free path is limited by the much longer recombination lifetimes of the order of microseconds. The same mechanism holds for the high secondary electron yield of diamond with NEA; electron yields as high as 85 have been reported.[12] In so-called electron amplifiers, a beam of high energy (up to 10 keV) primary electrons impinging on the back surface of a thin (0.5 mm) hydrogenated diamond results in

Dr. K. M. O'Donnell
Australian Synchrotron
Clayton, Victoria 3168, Australia
E-mail: kane.odonnell@synchrotron.org.au
M. T. Edmonds, Dr. C. I. Pakes
Department of Physics
La Trobe University
Victoria 3086, Australia
Prof. J. Ristein, Prof. L. Ley
Lehrstuhl für Technische Physik
Erlangen 91058, Germany
Dr. A. Tadich, Dr. L. Thomsen
Australian Synchrotron
Clayton, Victoria 3168, Australia
Dr. Q.-H. Wu
Department of Chemistry
College of Chemistry and Life Science
Quanzhou Normal University
Quanzhou 362000, China

DOI: 10.1002/adfm.201301424

the emission of thermalized electrons at the front surface that exceeds the primary current by factors up to 300.[2]

The wide spectrum of applications for diamond NEA surfaces raises questions about the stability of the H termination and whether or not there are other means to induce NEA on diamond. In ultrahigh vacuum (UHV), hydrogen is stable up to at least 800 °C on account of the strong covalent C–H bond. However, in the presence of oxygen or water, C–H bonds are replaced by C–O or C–OH bonds, and in air that happens within seconds at 200 °C and the NEA is lost. Hence, there are numerous reports of diamond NEA surfaces induced by metals or small molecules deposited onto the surface.[13–15] In none of these reports has the actual value of the EA been measured. Instead, they rely on the position of the low energy cut-off in the distribution of inelastically scattered secondary electrons in a UV-excited photoemission experiment. The cut-off energy E_{CUT} is determined by the highest barrier imposed on secondary electron emission from the sample and it coincides with E_{VAC} for surfaces with PEA. As the electron affinity χ drops so does E_{CUT} until $\chi = 0$, when E_{VAC} and CBM coincide. When E_{VAC} is further lowered ($\chi < 0$), E_{CUT} remains pinned at CBM. Hence, even when this last condition is fulfilled, there is no guarantee that the surface really has a negative EA. Only if the cut-off at CBM is accompanied by a large (of the order of a factor of 100) increase in the secondary electron yield right at cut-off is there an additional indicator of NEA for the reasons mentioned above. Since that is not observed in any of these reports, it remains doubtful whether true NEA rather than an EA close to zero was actually achieved.

Recently, on the basis of electronic structure calculations, O'Donnell et al. have suggested that a lithiated and oxidized diamond surface should exhibit a substantial negative EA of up to −3.9 eV.[16] Here, we show that one can generate a NEA surface with excellent secondary electron yield enhancement using a simple activation procedure involving lithium and elevated temperature on oxidized diamond. We use photoelectron spectroscopy (PES) with a synchrotron radiation source to demonstrate that the thermally activated Li-diamond surface exhibits the high secondary electron yield typical of a NEA surface, as well as to characterize the chemical changes of the surface as a function of the activation process. Unequivocal proof for the presence of a negative electron affinity is demonstrated using total photoelectron yield spectroscopy (TPYS). The surface properties are shown to be robust against the absorption of additional Li and exposure to ambient conditions.

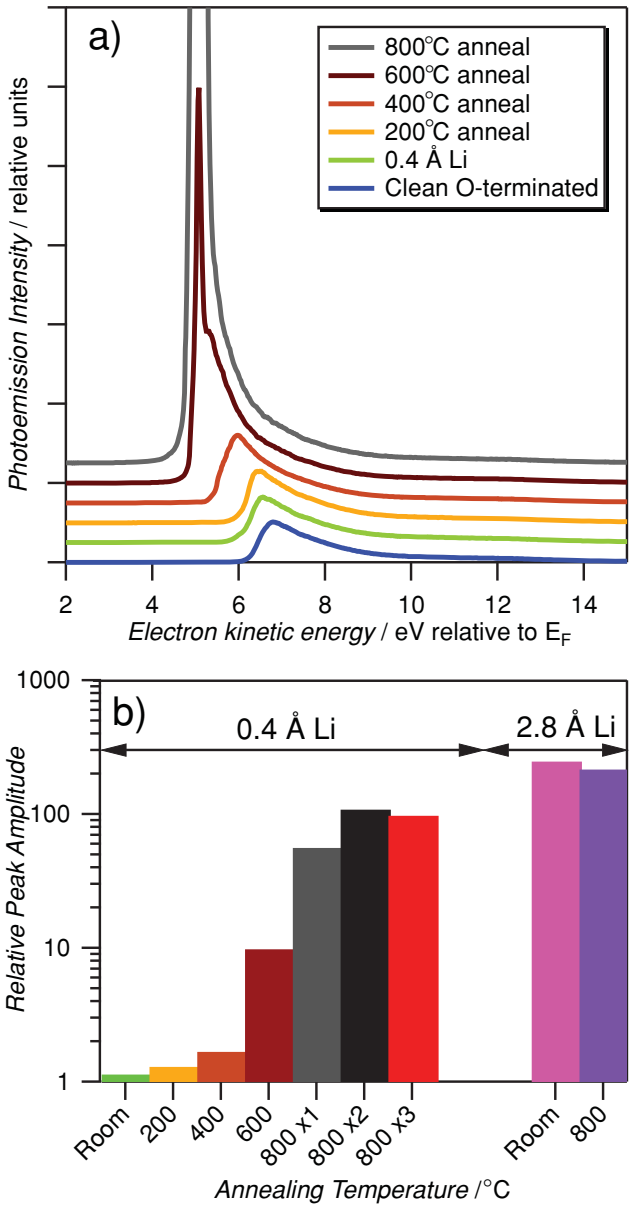

Figure 1. a) Change in low kinetic energy secondary electron spectrum with annealing. The 400 °C spectrum shows a marked shift to lower energies and a slight shape change. The first sign of the signature NEA peak is after the 600 °C anneal. After the 800 °C anneal, the NEA peak is so large that the original secondary electron spectrum is completely obscured. The peak of the 800 °C anneal is cut off in the Figure to allow the progression of the other peaks to be visible. b) The secondary electron peak amplitude of each data set in the annealing cycle, showing the effect of repeated annealing. Note the logarithmic scale.

2. Results and Discussion

2.1. Low Kinetic Energy Electron Spectra and Total Photoyield

A series of low kinetic energy (KE) electron spectra, which represent the energy distribution of inelastically scattered secondary electrons as they are emitted from a plasma oxidized (100) diamond sample, appear in **Figure 1**a. The figure shows the progression from a PEA to NEA state for a sample that was covered with 0.4 Å of lithium and annealed at progressively higher temperatures. The clean and 0.4 Å Li covered surfaces have a very similar low KE spectrum, with a low energy cut-off that lies 6.4 eV above the Fermi energy E_F, in excellent agreement with a previously published value of 6.3 eV for the C(100)–(1 × 1):O surface.[10] Starting with an annealing temperature of 400 °C the low energy cut-off moves to lower kinetic energies, indicating a reduction in work function. After a 600 °C anneal for 15 min, the cut-off energy is lowered by a total of 1.4 eV

Table 1. Summary of the changes in low kinetic energy secondary electron spectra upon lithium deposition and annealing.

Lithium Coverage [Å]	Cut-off energy[a] $E_{CUT} - E_F$ [eV]	Relative Secondary Electron Peak Amplitude	Relative Secondary Electron Integrated Intensity
Clean	6.4	1.0	1.0
0.02 Å Li	6.5	1.0	1.0
0.03 Å Li	6.5	1.0	1.0
0.05 Å Li	6.5	1.2	1.0
0.07 Å Li	6.4	1.1	1.1
0.08 Å Li	6.4	1.1	1.0
0.1 Å Li	6.4	1.1	1.1
0.4 Å Li	6.3	1.1	1.1
200 °C anneal, 15 min	6.2	1.3	1.2
400 °C anneal, 15 min	5.6	1.7	1.5
600 °C anneal, 15 min	5.0	9.5	3.0
800 °C anneal, 15 min	*4.9*	55.6	9.6
800 °C anneal, 30 min (total)	*4.6*	108.5	20.7
800 °C anneal, 60 min (total)	*4.7*	96.9	18.6
2.8 Å Li	*4.0*	248.0	74.3
800 °C anneal, 15 min	*4.6*	216.3	43.0

[a]The cut-off is defined as the energy at half-maximum on the low kinetic energy side of the spectrum, relative to the Fermi level. This is done so as to take the finite spectral resolution into account. Values in italics cannot be regarded as a measure of the sample workfunction. The uncertainty in these values is ±0.1 eV.

to $E_{CUT} - E_F = 5.0$ eV and the spectrum changes dramatically with a very intense and narrow (0.16 eV) peak appearing at the low energy cut-off position. Three further annealing steps at 800 °C increase the amplitude of the low energy peak further by over two orders of magnitude compared to the original surface as demonstrated in Figure 1b. We take that as a first indication that the lithium-covered oxygenated diamond surface is "activated" to a state of NEA by annealing above 600 °C. The value of the secondary electron cut-off relative to E_F and the relative yield (both peak amplitude and integrated intensity) of secondary electrons as function of lithium deposition and annealing are summarized in **Table 1**.

In order to understand the changes in the spectra seen in Figure 1, we must consider the position of the bands, the Fermi level, and vacuum level for this particular surface. These are illustrated for the three cases of PEA, effective negative electron affinity, and true NEA in **Figure 2**. In our experiment, we know the position of the Fermi level and the surface band bending from core level spectra discussed later in the paper and in the Experimental Section. Relevant for the present is the result that the value of $E_F - E_{VBM} = (0.9 \pm 0.1)$ eV at the surface was found to be constant in our experiment, regardless of lithium deposition or annealing. Combined with the bulk Fermi level position of our B-doped sample of (0.20 ± 0.05) eV above the valence-band maximum (VBM), this corresponds to an unchanging downward band bending of (0.7 ± 0.2) eV. With the band gap of $E_G = 5.5$ eV for diamond, this implies that as long as $E_{CUT} - E_F > E_G - 0.9$ eV, the surface has PEA and $E_{CUT} - E_F = \varphi$, the workfunction. For a PEA emitter, the vacuum level is substantially above the CBM and presents the barrier to escaping electrons, as discussed earlier. This results in a broad inelastic spectrum sharply cut-off at the vacuum level, as shown in Figure 2a. In this case, one can determine the electron affinity of the surface according to $\chi = \varphi + (E_F - E_{VBM}) - E_{GAP}$. For the surface prior to lithium deposition, this gives a positive electron affinity of (1.8 ± 0.1) eV, in good agreement with the results of Maier et al.[10]

Once the vacuum level moves below the CBM at the surface, $E_{CUT} - E_F$ is pinned at the position of the CBM at the surface and neither the workfunction nor the electron affinity can be related to E_{CUT}. The surface is in a state of "true" NEA. The thermalized electrons are now able to escape and form a narrow and intense peak at low kinetic energies, as shown in Figure 2c. The low kinetic energy spectra for the 800 °C annealed sample is representative of this structure. The peak amplitude is much larger (56 times larger than for the clean surface), with a full-width half-maximum of 0.3 eV, reflecting full emission from the CBM. At the same time, the cut-off energy E_{CUT} has dropped to its limiting value of (4.6 ± 0.1) eV. Further annealing was found to increase the yield even further as did deposition of more lithium (Figure 1b).

In the case where the electron affinity falls in the range $0 < \chi < 0.7$ eV, the vacuum level lies above the CBM at the surface but below the bulk position of the CBM. This corresponds to the situation of effective NEA (Figure 2b). In this case, one expects to see a fraction of electrons that are not fully thermalized to the CBM at the surface escape from the CBM by tunneling, within the space charge region. The sharp low energy cut-off is still determined by the vacuum level, whereas the exponentially decreasing tunneling probability as one moves up in energy results in a

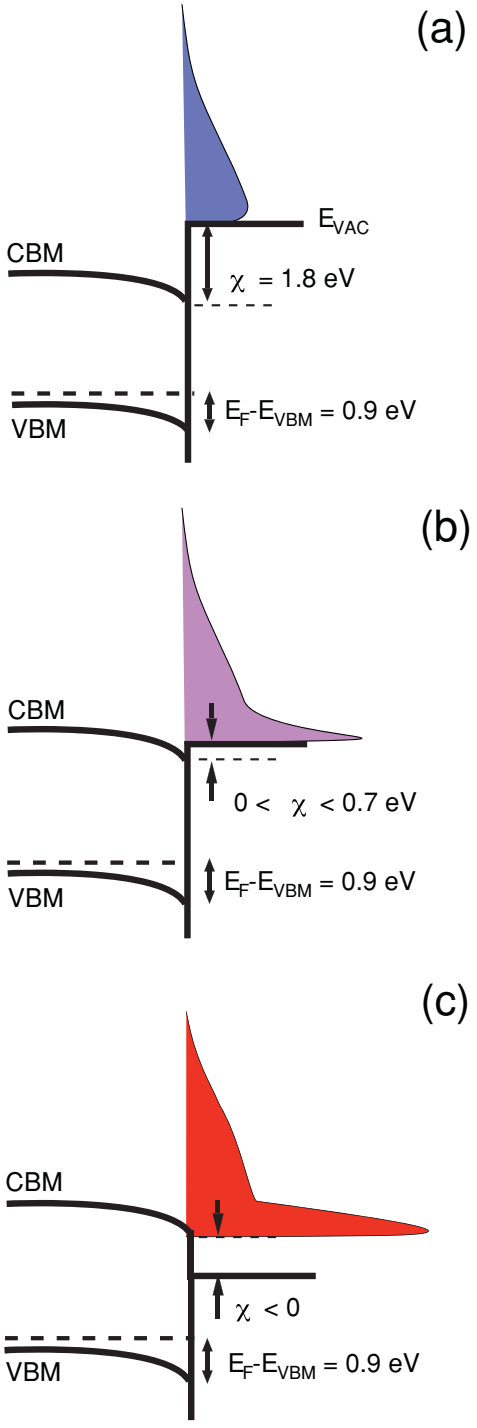

Figure 2. Band diagram and expected secondary electron emission spectrum for three cases of electron affinity, a) positive electron affinity (PEA), b) effective negative electron affinity where the vacuum level is above the CBM at the surface but below the CBM in the bulk, and c) true NEA, where the vacuum level is below the conduction band minimum at the surface. The emission spectra are schematic and do not reflect the broadening due to finite experimental resolution.

particularly narrow peak width. This is the situation we observe after 600 °C annealing as seen in Figure 1a. The cut-off E_{CUT} = 5.0 eV corresponding to χ = 0.4 eV falls within the window of

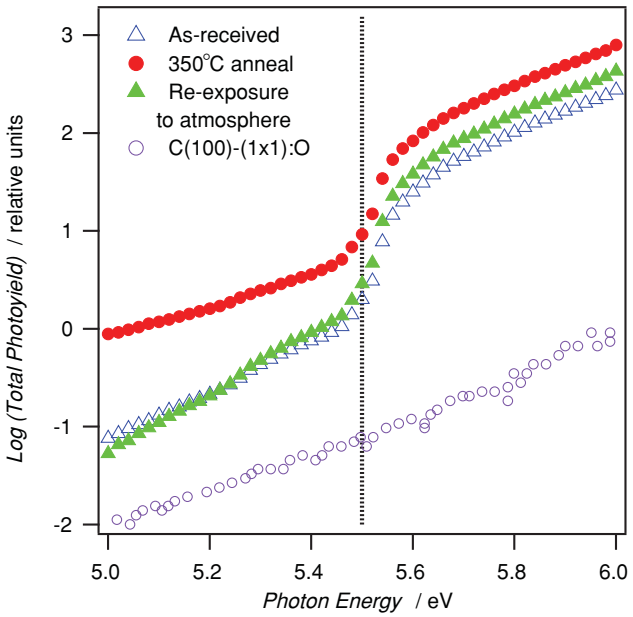

Figure 3. Total photoyield for the diamond sample as a function of photon energy. The vertical line indicates the experimental indirect bandgap of diamond (5.5 eV). A comparison to a bare oxygenated surface (found in the literature)[31] illustrates the difference between NEA and PEA surfaces.

effective NEA, as defined above. Indeed, we find that, unlike the peak widths of about 0.3 eV seen for the case of true NEA, the width here is only about 0.16 eV, a considerably narrower value.

To demonstrate unequivocally that the surface exhibits NEA, a total photoyield spectroscopy (TPYS) measurement was performed, that is, the total number of photoemitted electrons per incident photon measured as a function of photon energy. For a NEA surface, there will be a clear onset in photoyield at the photon energy equal to the band gap of 5.5 eV, with the yield spectrum resembling the absorption coefficient of diamond.[8,11] In our case, TPYS measurements were carried out at the University of Erlangen, necessitating the removal of the sample from vacuum for shipping. The sample was stored under argon and it is estimated that it was exposed to air for approximately 5–10 min before measurement. **Figure 3** shows the results of TPYS measurements for the original air-exposed sample, for the same sample after annealing at 350 °C in UHV for 30 min, and finally after re-exposure to air for 5 min. For all three spectra, the jump in photoyield at the diamond band gap energy is observed, which is a clear sign of NEA. After annealing, the total electron yield above the bandgap is 2–3 times greater because of the removal of electron-attenuating airborne adsorbates. Nevertheless, this increase is substantially smaller than the orders of magnitude increase observed for samples where NEA is achieved by hydrogen-termination of diamond.[17] In this case, exposure to air leads to p-type surface conductivity as a result of surface transfer doping;[18] this is accompanied by upward band bending that constitutes an additional barrier for electron emission that is removed together with the surface conductivity after annealing in vacuum. For the lithiated diamond considered here, the fact that we do not see a large reduction in total photoyield upon atmospheric

exposure suggests that transfer doping and the concomitant upward band bending which reduces the electron yield does not occur; this was confirmed by an electrical measurement on an identically prepared intrinsic diamond sample which showed no sign of p-type surface conductivity. It is unclear why there is apparently no surface transfer doping and we are led to speculate that either the energy level alignment is unfavoured for charge transfer or whether the presence of surface states has pinned the Fermi level to prevent band bending. The apparent absence of transfer doping on the lithiated surface is the subject of further investigation. In any case, the small change in photoyield after atmospheric exposure indicates a significant degree of air stability, making the lithiated diamond surface potentially far more useful for applications involving poor vacuum as, for example, in image intensifier tubes or field emission devices.

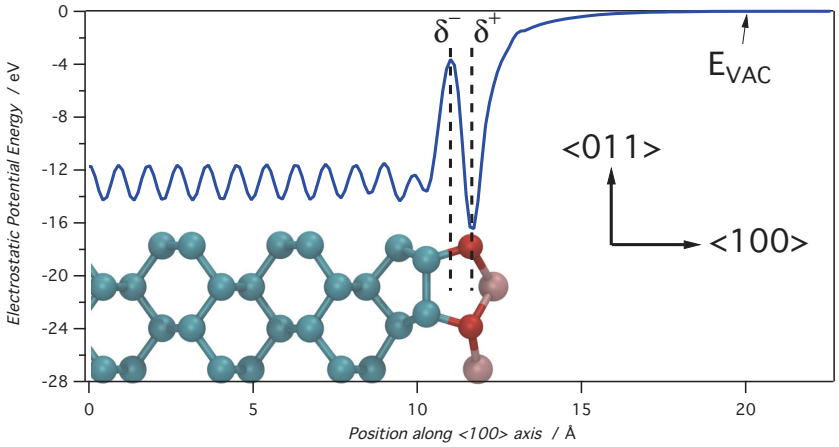

Figure 4. Computed electrostatic potential energy for the ideal lithiated and oxidized diamond (100) surface. The large surface dipole apparent in the potential is projected onto the structure diagram showing that the dipole is not atom-centered between the Li and O species as might be expected.

2.2. Core Level Spectroscopy and Surface Chemistry

To elucidate details about the surface chemistry before and after lithium deposition and annealing, we use core-level photoelectron spectroscopy. A negative electron affinity surface is expected to have a significant surface dipole. The electrostatic potential due to the dipole will cause the core levels of the surface species to shift in addition to the ordinary core level shifts caused by the charge transfer involved in chemical bonding. Our calculations[16] suggest that the ideal C(100)–(1 × 1):LiO surface has a large dipole indeed. **Figure 4** shows the calculated plane-averaged electrostatic potential through the C(100)–(1 × 1):LiO surface with the atomic positions overlaid. Unlike the hydrogenated diamond surface, the C(100)–(1 × 1):LiO surface dipole is not atom-centered and the Li–O bonds are not sufficiently normal to the surface to induce such a dipole. Instead, there is a delocalization of surface charge caused by the lowering of electronic states in the presence of the positive Li ion. The result is that the lithium and oxygen sites sit within the positive side of the surface dipole. The negative side of the dipole is located between the oxygen and first layer carbon sites. Therefore, we expect that both the O 1s and Li 1s core levels will be increased in binding energy due to attractive potential associated with the positive side of the surface dipole. In addition to this, the component of the O 1s spectrum related to Li–O bonding will be shifted to a relatively lower binding energy due to charge transfer from the Li.

In light of this potential environment, we can interpret the core level spectra. **Figure 5** shows a series of surface-sensitive C 1s (column a), O 1s (column b), and Li 1s (column c) core-level spectra obtained for (from bottom to top) i) the oxygen-terminated surface after annealing in UHV, ii) followed by Li deposition of 0.4 Å, iii) followed by 3 cycles of annealing at 800 °C for a total time of one hour, and iv) after further lithium deposition to 2.8 Å and a subsequent 800 °C anneal.

The C 1s peak (Figure 5a) shows the expected bulk diamond peak at 284.8 eV (labelled CA) with side peaks at 285.8 eV (CB1), 286.8 eV (CB2), and 284.0 eV (CC). The binding energy of the bulk component (CA) does not change as a function of surface treatment. Using the known VBM to bulk C 1s core level energy difference of 283.9 eV,[10] we can compute the surface $E_F - E_{VBM}$ = (0.9 ± 0.1) eV that does not change over the whole range of experimental conditions. We associate peaks CB1/2 with surface carbon-oxygen bonding, likely dominated by C–O–C (ether-bridge) and C=O (carbonyl) groups.[19–21] Peak CC is likely from surface dimer carbons which have an increased sp^2 character compared to bulk diamond.[22] At 330 eV, the inelastic mean free path in diamond is approximately 3–5 Å,[23,24] agreeing well with our measured bulk to surface ratio of approximately 1:1. From the ratio of the areas of the surface components, we estimate a fraction of 33% of the surface carbon atoms to be oxygenated.

The clean oxygenated surface has a simple O 1s core level spectrum (Figure 5b) dominated by a single peak at 531.6 eV (peak OA) characteristic of a double-bonded oxygen species such as C=O or C–O–C. Upon 0.4 Å lithium adsorption, the O 1s peak decreases in area by 20%, suggesting that lithium adsorbs over the oxygen-terminated regions. The Li 1s core level after 0.4 Å lithium deposition shown in Figure 5c exhibits a single peak at 55.4 eV, slightly higher than for metallic lithium (54.8 eV).[25] Prior to annealing, however, there is little evidence in the core level spectra of a change in surface dipole due to lithium adsorption, which is consistent with the positive electron affinity at this point discussed earlier in conjunction with Figure 1.

Annealing alters the shape of the core level spectra and induces shifts consistent with a change in the surface dipole. After annealing at 800 °C for a total annealing time of one hour, when NEA is firmly established on the surface, both the O 1s and Li 1s spectra shift rigidly by 0.9 and 0.7 eV, respectively, to higher binding energies. The large rigid shift to higher binding energy for the O 1s spectrum is consistent with the surface oxygen and lithium residing within a lowered electrostatic

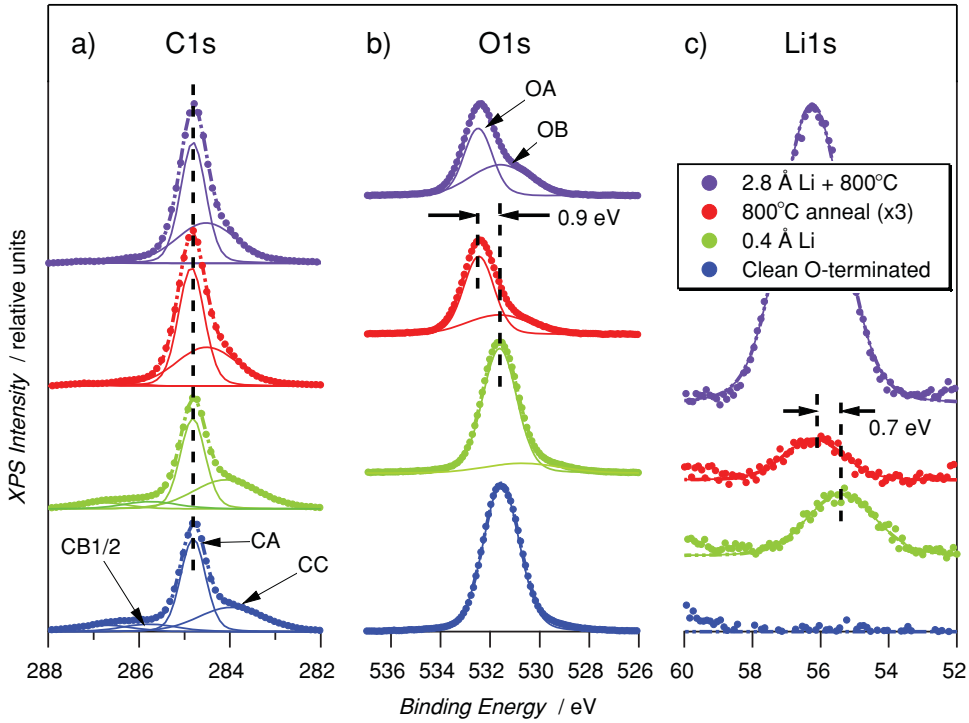

Figure 5. a) C 1s core level taken at 330 eV photon energy. b) O 1s core level taken at 700 eV. c) Li 1s core level taken at 150 eV. Due to the difference photon energies used for each core level, the peak heights are not comparable across species here.

potential as expected from Figure 4. The concomitant appearance of a prominent side peak (OB) at 0.8 eV lower binding energy with lithium deposition after annealing indicates the formation of ionic Li–O bonds and is consistent with negative charge transfer from lithium to oxygen as expected. The change in the ratio of peak OA to peak OB is also significant. Although low temperature annealing (400 °C, not shown in Figure 5) reduces the overall amount of oxygen on the surface, further anneals at higher temperature do not reduce the quantity of oxygen present but instead peak OB increases at the expense of peak OA. We associate this with the activation process, causing a structural and chemical change to a more ordered lithium-oxygen bonding arrangement that induces the surface dipole leading to a state of NEA.

From these observations, we conclude that activation is a necessary process to provide a structural change leading to NEA. Our previous calculations show that the oxygenated surface allows a large number of metastable lithium bonding sites that do not exhibit a large surface dipole. Therefore, it is likely that upon adsorption of lithium, lithium atoms move into these metastable configurations. Annealing will then enable a structural shift to the thermodynamically preferred state seen in Figure 4. Ether-bridge C–O–C structures and carbonyl C=O structures are chemically stable; thus, the structural shift must involve the breaking of a C–O bond to give C–O–Li–O–C structures as is signaled by the appearance of the chemically shifted component OB in Figure 5.

Once activated, the NEA state of the surface is preserved under exposure to more lithium. It is clear from the peak OA/OB ratio that 0.4 Å Li coverage is not enough for monolayer coverage. It follows that adding more lithium should increase the surface dipole and electron yield. This prediction is born out in the secondary electron yield data shown in Figure 1b and Table 1, as well as the core level spectra. In Figure 5, it can be seen that with 2.8 Å lithium deposited and annealed, feature OB in the O 1s spectrum increases to 50% of the total O 1s area, supporting our assignment of OB to Li–O bonding.

The situation for the C 1s peak is more complicated because there will be three components that move independently: i) a bulk C 1s component that is not affected by the surface dipole and should not move unless the band bending changes, ii) surface carbons bonded to oxygen, normally higher in binding energy than the bulk C 1s peak but will move lower in binding energy due to the negative side of the surface dipole, and iii) surface carbons not bonded to oxygen which, as surface atoms, should be on the positive side of the surface dipole and should move to higher binding energy. The result is that for carbon the components should all merge towards each other, as observed in Figure 5a.

3. Conclusions

In the present work, we have demonstrated that lithiated, oxygenated diamond can be activated to yield a NEA surface with excellent secondary electron emission properties. Photoelectron spectroscopy indicates that the lithium bonds to the oxygen-terminated regions of the diamond and, after annealing at high temperatures, induces a structural change to a surface with a large surface dipole. The NEA is highly resilient to

high-temperatures and even atmospheric exposure. We therefore suggest that lithium-deposited oxygenated diamond is an ideal basis for technological applications involving electron emission, including field emitters, current amplifiers, image intensifiers, and solar blind photocathodes.

4. Experimental Section

Sample Preparation: The substrate for all our experiments was a type-IIa C(100) crystal sourced from Element 6, with surface roughness better than 5 nm. A 300 nm epitaxial boron-doped overlayer was grown on the substrate by chemical vapor deposition (CVD), the conductivity of the B-doped layer eliminating charging effects during photoemission measurements. Low energy electron diffraction (not shown) gave a sharp (1×1) pattern as expected for oxygen-terminated diamond and shows the epitaxial overlayer preserves the underlying (100) structure with good surface crystallinity. The position of the Fermi level with respect to the bulk valance band maximum can be determined from the energy of the boron acceptor and the boron concentration to be (0.20 ± 0.05) eV. This gives constant band bending of approximately (0.7 ± 0.2) eV. Such a value is consistent with previous results for oxygenated diamond.[10] The sample was cleaned by boiling in sulphuric and nitric acids, then oxygen-terminated by exposure to an oxygen plasma for 5 min. The sample was mounted in a Ta envelope onto a holder with an underlying boron nitride heater for sample annealing in UHV. A thermocouple was connected to the surface of the sample holder underneath the Ta envelope and was used to measure the temperatures quoted here.

Lithium was deposited using a thoroughly degassed SAES getter source. The background pressure in the preparation chamber was below 2×10^{-10} mbar. The amount of Li deposited was determined by the Li 1s core level peak area as measured using X-ray photoelectron spectroscopy (XPS); a series of depositions using a constant deposition rate was performed for increasing times, with the measured XPS peak intensities fitted to a simple overlayer attentuation model:

$$I_t = I_b\,(1 - \exp(-Rt/(\lambda \cos\theta))) \quad (1)$$

where I_t is the Li 1s peak area after a given deposition time t, I_b is the intensity expected for bulk lithium, R is the deposition rate, $\lambda = 7$ Å[26] is the inelastic mean free path at the kinetic energy of the photoelectrons under consideration, and $\theta = 10°$ is the angle between the detector and the surface normal. Fitting Equation 1 to the core level peak areas yields the values of I_b and $R = (0.20 \pm 0.05)$ Å min^{-1}, in our case. By analogy with the results of Petrick and Benndorf,[27] we expect a sticking coefficient close to unity in the present case.

Photoelectron Spectroscopy: Photoelectron spectroscopy was carried out using the soft X-ray spectroscopy beamline at the Australian Synchrotron with a typical total energy resolution of better than 100 meV[28]. The base pressure during measurements was less than 1.0×10^{-10} mbar. Photon energies were chosen to ensure maximum surface sensitivity for the oxygen, carbon, and lithium core levels and, in the case of lithium, to optimize the X-ray photoionization cross-section. The photon energies used were 700 eV for the O 1s core level, 330 eV for the C 1s core level, and 150 eV for the Li 1s core level and the low kinetic energy secondary electron spectra. All binding energies are referenced to the Fermi level, as determined after every change in photon energy by setting the 4f 7/2 core level binding energy of a Au sample in electrical contact with the sample to 84.00 eV. The photon flux was continually monitored using the drain current from a 50% transmissive gold mesh, allowing intensity normalization across different scans. A Shirley background was subtracted from each data set before peak fitting.[29] Peaks were fitted with Fityk[30] using Voigt profiles with a fixed Lorentzian width of 0.15 eV reflecting the core-hole lifetime,[22] and a variable Gaussian width. For the low kinetic energy spectra, a negative bias in the range 6–10 V was applied to the sample to overcome the workfunction of the analyzer and ensure transmission and collection of the lowest energy electrons. The actual applied bias was measured using the shift in core levels with and without the bias, allowing the low kinetic energy spectra to be referenced to the system Fermi level with the bias subtracted.

Acknowledgements

The authors acknowledge the technical support of B. Cowie for help with the low kinetic energy measurements at the Australian Synchrotron. This work was supported by the Multi-modal Australian ScienceS Imaging and Visualisation Environment (MASSIVE) (www.massive.org.au).

Received: April 26, 2013
Published online: June 3, 2013

[1] K. Okano, S. Koizumi, S. Silva, G. Amaratunga, *Nature* **1996**, *381*, 140.
[2] X. Chang, Q. Wu, I. Ben-Zvi, A. Burrill, J. Kewisch, T. Rao, J. Smedley, E. Wang, E. Muller, R. Busby, D. Dimitrov, *Phys. Rev. Lett.* **2010**, *105*, 164801.
[3] J. W. Schwede, I. Bargatin, D. C. Riley, B. E. Hardin, S. J. Rosenthal, Y. Sun, F. Schmitt, P. Pianetta, R. T. Howe, Z.-X. Shen, N. A. Melosh, *Nat. Mater.* **2010**, *9*, 1.
[4] F. Köck, J. Garguilo, B. Brown, R. J. Nemanich, *Diamond Relat. Mater.* **2002**, *11*, 774.
[5] R. L. Bell, *Negative electron affinity devices*, Clarendon Press, Oxford, **1973**.
[6] W. E. Spicer, *Appl. Phys.* **1977**, *12*, 115.
[7] F. Himpsel, J. Knapp, J. Van Vechten, D. Eastman, *Phys. Rev. B* **1979**, *20*, 624.
[8] C. Bandis, B. Pate, *Phys. Rev. Lett.* **1995**, *74*, 777.
[9] J. B. Cui, J. Ristein, L. Ley, *Phys. Rev. Lett.* **1998**, *81*, 429.
[10] F. Maier, J. Ristein, L. Ley, *Phys. Rev. B* **2001**, *64*, 165411.
[11] J. B. Cui, J. Ristein, L. Ley, *Phys. Rev. B* **1999**, *60*, 16135.
[12] A. Shih, J. Yater, P. Pehrsson, J. Butler, C. Hor, R. Abrams, *J. Appl. Phys.* **1997**, *82*, 1860.
[13] P. Baumann, R. J. Nemanich, *Appl. Surf. Sci.* **1996**, *104*, 267.
[14] O. Küttel, O. Gröning, E. Schaller, L. Diederich, P. Gröning, L. Schalpabach, *Diamond Relat. Mater.* **1996**, *5*, 807.
[15] K. W. Wong, Y. Wang, K. Lee, R. Kwok, *Diamond Relat. Mater.* **1999**, *8*, 1885.
[16] K. M. O'Donnell, T. Martin, N. Fox, D. Cherns, *Phys. Rev. B* **2010**, *82*, 115303.
[17] D. Takeuchi, M. Riedel, J. Ristein, L. Ley, *Phys. Rev. B* **2003**, *68*, 041304.
[18] F. Maier, M. Riedel, B. Mantel, J. Ristein, L. Ley, *Phys. Rev. Lett.* **2000**, *85*, 3472.
[19] M. Hossain, T. Kubo, T. Aruga, N. Takagi, T. Tsuno, N. Fujimori, M. Nishijima, *Surf. Sci.* **1999**, *436*, 63.
[20] K. Loh, X. Xie, Y. Lim, E. Teo, J. Zheng, T. Ando, *Surf. Sci.* **2002**, *505*, 93.
[21] A. Laikhtman, A. Lafosse, Y. Le Coat, R. Azria, A. Hoffman, *J. Chem. Phys.* **2003**, *119*, 1794.
[22] R. Graupner, F. Maier, J. Ristein, L. Ley, C. Jung, *Phys. Rev. B* **1998**, *57*, 12397.
[23] B. Pate, *Surf. Sci.* **1986**, *165*, 83.
[24] J. F. Morar, F. J. Himpsel, G. Hollinger, J. L. Jordan, G. Hughes, F. R. McFeely, *Phys. Rev. B* **1986**, *33*, 1340.
[25] J. Hoenigman, R. Keil, *Appl. Surf. Sci.* **1984**, *18*, 207.
[26] C. J. Powell, A. Jablonski, *NIST Electron Inelastic-Mean-Free-Path Database, Version 1.2, SRD 71*, National Institute of Standards and Technology, Gaithersburg **2010**.
[27] S. Petrick, C. Benndorf, *Diamond Relat. Mater.* **2001**, *10*, 519.
[28] B. C. C. Cowie, A. Tadich, L. Thomsen, *AIP Conf. Proc.* **2010**, *1234*, 307.
[29] D. A. Shirley, *Phys. Rev. B* **1972**, *5*, 4709.
[30] M. Wojdyr, *J. Appl. Crystallogr.* **2010**, *43*, 1126.
[31] P. Strobel, *PhD Thesis*, University of Erlangen, Germany **2008**.